Evolution of Multicomponent [Pd$_2$ABCD] Cages

Kai Wu,[1,2] Elie Benchimol,[1] Ananya Baksi[1,3] and Guido H. Clever[1]*

[1]Department of Chemistry and Chemical Biology, TU Dortmund University, Otto-Hahn-Str. 6, 44227 Dortmund, Germany.
[2]Present address: Department of Chemistry, University of Cambridge, Lensfield Road, Cambridge, CB2 1EW, UK.
[3]Present address: Department of Chemistry, Jadavpur University, Kolkata-700032, West Bengal, India.
*e-mail: guido.clever@tu-dortmund.de

ABSTRACT: Synthetic supramolecules, inspired by biological hosts, catalysts and machines, promise to find application in sustainable synthesis, separation, energy conversion and medicine. However, the implementation of multiple functionalities within distinct self-assembled structures still poses considerable challenges. In particular metal-mediated assemblies are difficult to form from multiple chemically different building blocks without falling into narcissistic self-sorting or a statistical mess. Here we report a systematic series of integratively self-assembled heteroleptic cages in which two square-planar Pd^{II} cations are bridged by four chemically different bis-pyridyl ligands **A**, **B**, **C** and **D** via a collection of synergistic effects to form a single isomer of lantern-shaped cage [Pd$_2$**ABCD**] as exclusive product. This ultimate self-sorting goal, forming just one out of 55 possible structures, is reached under full thermodynamic control and can be realized progressively (by combining heteroleptic progenitors such as [Pd$_2$**A**$_2$**C**$_2$] with [Pd$_2$**B**$_2$**D**$_2$]), directly from ligands and Pd^{II} cations, or – most impressively – by mixing all four corresponding homoleptic cages. Structural and mechanistic details were comprehensively examined by NMR and mass spectrometry and nine single crystal X-ray structures. The rational design of complex multicomponent assemblies, formed in high yield under thermodynamic control, allows to incorporate different chemical moieties in a modular approach and advance the application level of functional nanosystems.

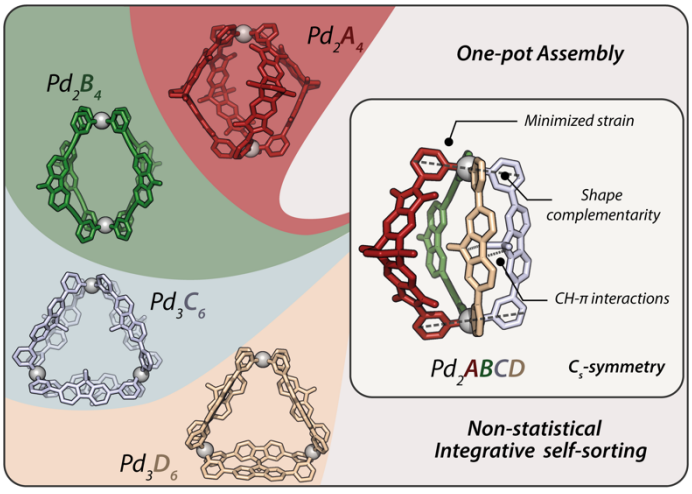

Biological systems have evolved precisely shaped nano-confinements of low symmetry for the selective recognition of C_1-symmetric substrates and their catalytic conversion[1]. Enzymes utilize folded peptide chains as scaffolds to precisely position and structurally support active elements such as binding sites and catalytic centers around defined cavities[2]. Inspired by these natural nano systems, synthetic chemists have developed supramolecular systems that resemble their biological paradigms, including both purely organic[3] and metal-mediated assemblies[4–6], to achieve molecular recognition and separation[7], reactive species stabilization[6,8], and confined catalysis[9]. In case of metallosupramolecular assemblies, further applicability can be achieved by using ligands equipped with dedicated functional units such as chiral groups[10], luminophores[11], redox centers[12,13] or photoswitches[14,15]. Nevertheless, a majority of reported examples consist of only one type of organic ligand per assembly, hence they are homoleptic, often have rather isotropic cavities, and overall high symmetries derived from Platonic or Archimedean solids, or the Goldberg polyhedra[16,17]. This may limit their application potential in advanced settings that require synergistic interplay of different ligand constituents, e.g. between recognition sites, catalytic moieties and chiral modulators. Multifunctional assemblies based on the contribution from two different components are still in their infancy, e.g. systems featuring circularly polarized luminescence (CPL) by intraassembly chirality transfer[18], charge-transfer in donor–acceptor systems[19], and cooperative catalysis[20–22]. In only few of the most complicated self-assembled systems reported to date, more than two differentiable functionalities, situated on separate components, have been involved[20,23,24].

Inspired by seminal investigations of Lehn[25], Sauvage[26], Fujita[27], Stang[28] and others[29], recent developments in the area of metallosupramolecular assembly have enabled the rational and clean combination of multiple building blocks in a non-statistical fashion. In this respect, the past several years have witnessed a rapid development of integrative self-sorting strategies to overcome entropic control and prevent the formation of statistical mixtures[30,31]. These include shape-complementary assembly (SCA)[32–36], charge-separation[20,28], templating effects[27,37], coordination sphere engineering (CSE)[38,39], the use of non-symmetric ligands[40,41], backbone steric hindrance[42], and carefully designed, multidentate donor environments[43].

Within the popular class of Pd^{II}-mediated structures, the lowest nuclearity, hence most simple, assembly with an accessible cavity is a lantern-shaped [Pd_2L_4] cage in which two square-planar cations are connected by four banana-shaped bis-monodentate pyridyl ligands. While most of the numerous reported examples are composed of a single type of ligand per assembly, recent studies by Crowley[39], Hooley[44], Zhang[45] and us[33] have shown that a proper choice of ligands allows to rationally combine two or – and this only via kinetic control – even

three, different ligands without creating statistical mixtures. Both from an entropic as well as chemical design point of view, the difficulty to achieve integrative self-sorting under thermodynamic control steeply increases when all four ligands that are sought to be combined are structurally different.

Results and discussion

In theory, without rational control, a supramolecular system consisting of four distinguishable bis-monodentate ligands **A**, **B**, **C**, and **D**, equally and independently able to coordinate to two square-planar Pd^{II} nodes, will lead to the formation of 55 different species (Supplementary Scheme 1), ranging from the simplest lantern-shaped homoleptic cages, e.g. $[Pd_2\mathbf{A}_4]^{4+}$, to multicomponent cages, e.g. $[Pd_2\mathbf{ABCD}]^{4+}$, with the highest complexity.

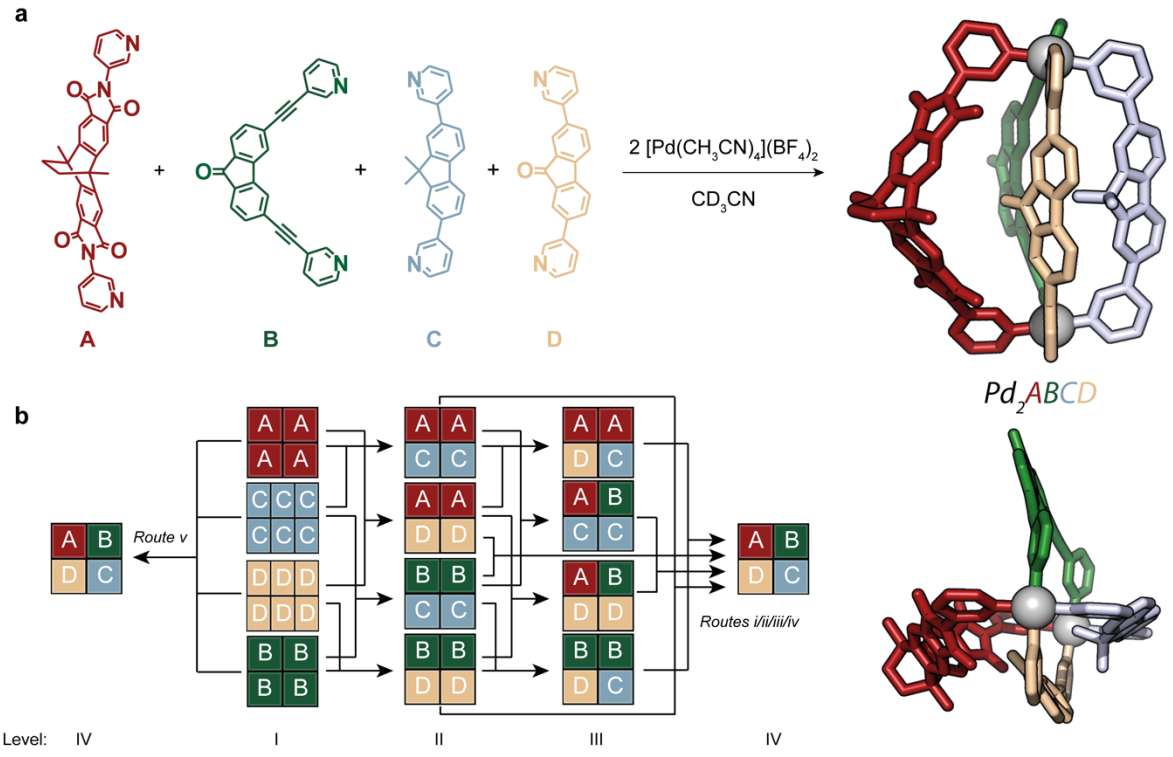

Fig. 1 | Self-assembly of heteroleptic multicomponent cage $[Pd_2\mathbf{ABCD}]^{4+}$ from four chemically different ligands. a, cage formation from ligands **A**, **B**, **C**, **D** and Pd^{II} (X-ray structure of $[Pd_2\mathbf{ABCD}]^{4+}$ depicted as side and top view). **b,** Evolution of complexity from homoleptic assemblies to the most complex heteroleptic assembly $[Pd_2\mathbf{ABCD}]^{4+}$ via different pathways.

Here we report the systematic construction of a new family of non-statistically assembled heteroleptic cages in which two square-planar Pd^{II} cations are bridged by up to four chemically

different ligands (Fig. 1). Ligand shape-complementarity, together with stabilizing C-H···π interactions and strain effects allow to reach this extreme level of integrative self-sorting. Our experiments show that the increase in complexity can be realized either progressively, by successive cage-to-cage transformations from homo- via two- and three-component heteroleptic cages, or directly by mixing either all ligand constituents with Pd^{II} or all four homoleptic cages. In the following, we compare these routes with the help of a comprehensive set of NMR and mass spectrometry results as well as nine single crystal X-ray structures of heteroleptic cages on the different complexity levels.

Heteroleptic cages with two different ligands

Recently, we reported that combining a pair of shape-complementary bis-monodentate ligands, i.e. carbazole-based ligand $\mathbf{B^0}$ and fluorene-based ligand **C**, with square-planar Pd^{II} cations in acetonitrile yields heteroleptic cage $[Pd_2\mathbf{B^0}_2\mathbf{C}_2]^{4+}$ through the SCA approach as single thermodynamic product[46]. Furthermore, by replacing ligand **C** with its fluorenone-based analogue **D**, carrying a central carbonyl group, analogue $[Pd_2\mathbf{B^0}_2\mathbf{D}_2]^{4+}$ was obtained exclusively in CD_3CN as proven by 1D, 2D NMR spectra and high-resolution electrospray ionization mass spectrometry (HR-ESI-MS; Supplementary Figs. 92 to 98). Similarly, by replacing ligand $\mathbf{B^0}$ with **B**, both heteroleptic cages $[Pd_2\mathbf{B}_2\mathbf{C}_2]^{4+}$ and $[Pd_2\mathbf{B}_2\mathbf{D}_2]^{4+}$ could also be obtained selectively (Supplementary Figs. 31 to 44). To control the rational introduction of three or four chemically different ligands, further shape-complementary ligand pairs needed to be explored. We previously reported that two Pd^{II} cations can bring four curved ligands **A** together to form an enclosed cavity, suitable for fullerene encapsulation[38]. Here we show that ligand **A** is also able to cleanly form heteroleptic cages $[Pd_2\mathbf{A}_2\mathbf{C}_2]^{4+}$ and $[Pd_2\mathbf{A}_2\mathbf{D}_2]^{4+}$ together with ligand **C** and ligand **D**, respectively. Indeed, both NMR and ESI MS studies as well as a single crystal X-ray structure of *trans*-$[Pd_2\mathbf{A}_2\mathbf{B}_2]^{4+}$ (Fig. 2a) clearly demonstrated the suitability of these ligand combinations for clean heteroleptic cage formation, both in solution and the solid state (Supplementary Figs. 52 to 63).

Heteroleptic cages with three different ligands

Next, we aimed to further increase the system's structural complexity by introducing a third differentiable ligand. Therefore, we carefully inspected ligands **C** and **D** – both complements of ligand **A** – and realized that although they share a similar backbone and the same pyridyl donor motifs, their electronic properties are distinguishable. Ligand **C** comprises a central dimethyl group, a potential C-H···π donor, while ligand **D**, presenting an unobstructed π-

surface, could act as a complementary acceptor. We thus suspected that the assembly of ligands **A**, **C**, and **D** with Pd^{II} will lead to a preferential interaction between neighbouring ligands **C** and **D** through integrative self-sorting[42]. This situation should energetically surpass the interaction between pairs of **C** or **D** in the competing assemblies $[Pd_2\mathbf{A}_2\mathbf{C}_2]^{4+}$ or $[Pd_2\mathbf{A}_2\mathbf{D}_2]^{4+}$. Indeed, the assembly of ligands **A**, **C**, and **D** with Pd^{II} in a 2:1:1:2 ratio in CD_3CN at 80 °C resulted in a well-resolved ^1H NMR spectrum (Fig. 3). ^1H DOSY experiment confirmed the formation of a single species, with a diffusion coefficient of 6.32×10^{-10} $m^2\,s^{-1}$, corresponding to a hydrodynamic radius of 1.0 nm (Supplementary Fig. 69), consistent with the size of a heteroleptic cage $[Pd_2\mathbf{A}_2\mathbf{CD}]^{4+}$. HR-ESI-MS provided convincing evidence for the expected stoichiometry by showing a series of peaks assigned to $[2Pd^{II}+2\mathbf{A}+\mathbf{C}+\mathbf{D}+nBF_4]^{(4-n)+}$ (n = 0–2; Supplementary Fig. 70). 2D NMR spectra were employed to assign all signals unambiguously and the correlation between proton H7 on ligand **C** (blue) and H7 on ligand **D** (yellow) allowed us to confirm the formation of a *cis*-configured $[Pd_2\mathbf{A}_2\mathbf{CD}]^{4+}$ cage (Supplementary Figs. 67 to 68). The two ligands **A** in the cage adjacent to ligands **C** and **D** are not equivalent anymore, thus resulting in two sets of NMR signals for ligand **A**.

Ultimately, the structure of cage $[Pd_2\mathbf{A}_2\mathbf{CD}]^{4+}$ was unambiguously confirmed by its X-ray crystal structure (Fig. 2b). Noteworthy, both ligands **A** were found to be direct neighbors, unlike their *trans*-arrangement seen in cage $[Pd_2\mathbf{A}_2\mathbf{B}_2]^{4+}$ (compare Figs. 2a and b). The dihedral angle $\angle\alpha$ between the two $[Pd(Py)_4]$ planes in the structure was measured to be 33.9°, indicating the presence of pronounced shape-complementarity, with **A** being the longer ligand opposite the two shorter ligands **C** and **D**[33]. As shown above, also ligand **B** can be a shape-complementary partner to both ligands **C** and **D**. We thus speculated that the exclusive formation of cage $[Pd_2\mathbf{B}_2\mathbf{CD}]^{4+}$ should also be feasible. Indeed, integrative self-sorting also proceeded when combining ligands **B**, **C**, **D** with Pd^{II}, yielding a similar NMR pattern and a characteristic HR-ESI-MS spectrum (Supplementary Figs. 45 to 51).

Next, we kept shorter ligands **C** and **D** as identical pairs and mixed these with **A** and **B** aimed at the formation of cages $[Pd_2\mathbf{ABC}_2]^{4+}$ and $[Pd_2\mathbf{ABD}_2]^{4+}$, respectively. A first glance, ligands **A** and **B** seem like they would not undergo obvious interactions, and we wondered if an integrative self-sorting would still be possible. Surprisingly, the mixture of ligands **A**, **B**, **C** and Pd^{II} in a stoichiometric ratio gave a well-resolved NMR spectrum with a similar pattern as observed for the heteroleptic cages described above. Again, HR-ESI-MS confirmed the clean formation of a cage with stoichiometry $[2Pd^{II}+\mathbf{A}+\mathbf{B}+2\mathbf{C}]^{4+}$ (Supplementary Figs. 71 to 77). Now, the two ligands **C** have different chemical environments, giving two sets of signals, and

the correlation between protons H7 and H7' of both ligands **C** allowed us to rule out the formation of a *trans*-configured cage (Supplementary Figs. 75). Likewise, the formation of cage $[Pd_2\mathbf{ABD}_2]^{4+}$ cage was achieved by replacing ligand **C** with **D** under otherwise same conditions (Supplementary Figs. 78 to 84).

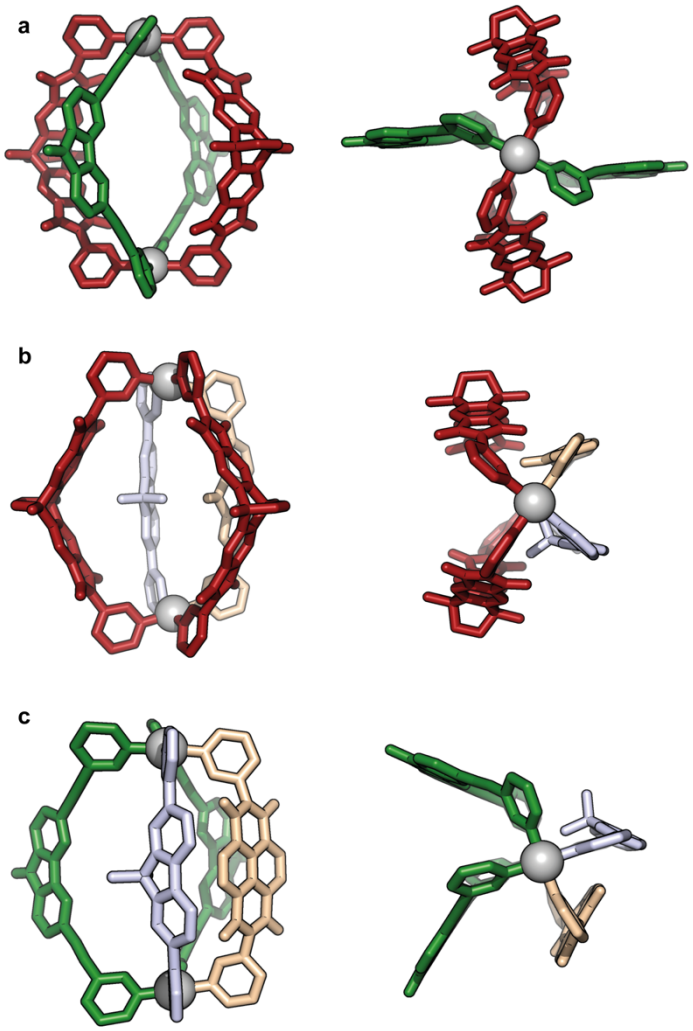

Fig. 2 | X-ray crystal structures of multicomponent heteroleptic cages with two or three different ligands. Side and top views of **a**, *trans*-$[Pd_2\mathbf{A}_2\mathbf{B}_2]^{4+}$; **b**, $[Pd_2\mathbf{A}_2\mathbf{CD}]^{4+}$ and **c**, $[Pd_2\mathbf{B}_2\mathbf{D}^4\mathbf{C}]^{4+}$ (counter anions, solvents and hydrogens omitted for clarity, further details see Supplementary Information).

Heteroleptic cages with four different ligands

Eventually, we set out to tackle the most challenging self-assembly, involving the simultaneous incorporation of four chemically different ligands. Remarkably, the combination of ligands **A**, **B**, **C**, and **D** with Pd^{II} in a 1:1:1:1:2 ratio in CD_3CN at 80 °C resulted in a complex, yet well-resolved, NMR spectrum (Fig. 3a). All the peaks belong to the same diffusion coefficient of 6.38×10^{-10} m^2 s^{-1} as calculated by a ^1H DOSY experiment, corresponding to a

hydrodynamic radius of 1.0 nm (Supplementary Fig. 90). The exclusive formation of a heteroleptic cage with sum formula $[Pd_2\mathbf{ABCD}]^{4+}$, featuring an unprecedented degree of integrative self-sorting, was verified by HR-ESI-MS, revealing a series of peaks assigned to $[2Pd^{II}+\mathbf{A}+\mathbf{B}+\mathbf{C}+\mathbf{D}+nBF_4]^{(4-n)+}$ (n = 0–2; Fig. 2c, Supplementary Fig. 91). The ^{1}H NMR spectrum revealed four sets of signals originating from the four different ligands and the integration values of protons H7 assigned to ligands **A**, **B**, **C**, and **D** gave a ratio of 1:1:1:1, also in line with the formation of the heteroleptic cage incorporating all the four ligands.

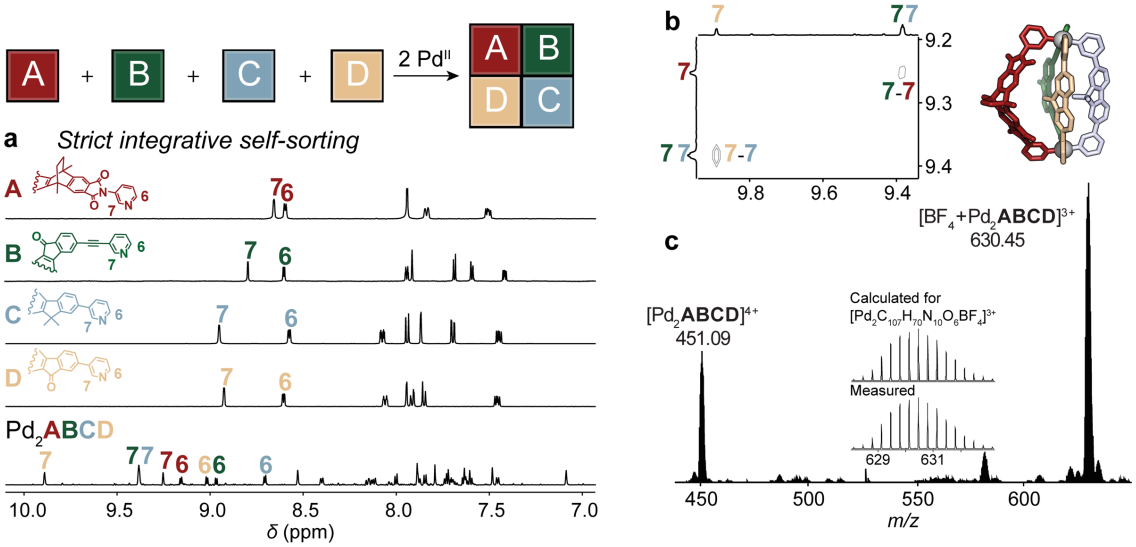

Fig. 3 | Characterization of heteroleptic multicomponent cage $[Pd_2\mathbf{ABCD}]^{4+}$. a, From top to bottom, ^{1}H NMR spectra (700 MHz, 298 K, CD_3CN) of **A**, **B**, **C**, **D**, $[Pd_2\mathbf{ABCD}]^{4+}$. **b,** Partial ^{1}H–^{1}H NOESY spectrum of $[Pd_2\mathbf{ABCD}]^{4+}$, revealing correlations between protons H7 of two ligand pairs. **c,** HR-ESI-MS of $[Pd_2\mathbf{ABCD}]^{4+}$ (isotopic pattern shown as inset).

By arranging four different ligands circularly around two metal nodes, three configurational isomers are possible (Fig. 4b). While mass spectrometry revealed the ligand stoichiometry, it could not answer which isomer is formed. From the results discussed above, we concluded that longer ligands **A** and **B** should be positioned in a *cis* relationship to each other. The same is true for shorter ligands **C** and **D** to allow for attractive interligand contacts and maximize the shape-complementary fit. Thus, a tentative $[Pd_2\mathbf{ADBC}]^{4+}$ isomer, carrying **A** and **B** in a *trans*-relationship, could be ruled out, leaving only two possible isomers, i.e. $[Pd_2\mathbf{ABCD}]^{4+}$ and $[Pd_2\mathbf{ABDC}]^{4+}$. NOESY correlations between protons H7 of ligands **A** and **B** and protons H7 of ligands **C** and **D** also support either of the latter two isomers (Fig. 3b), however, no correlations could be found between protons H7 of ligands **A** and **C** or **D** to distinguish these two isomers, leaving single-crystal X-ray structural analysis as the only option to solve this

question. Single crystals suitable for diffraction were obtained by vapor diffusion of benzene to the cage solution in CD_3CN. Structural analysis confirmed the formation of the $[Pd_2\mathbf{ABCD}]^{4+}$ isomer. The cage crystallizes in the $P\bar{1}$ space group, with the asymmetric unit containing one cage molecule (Fig. 1). The Pd···Pd distance in the structure is 13.67 Å, comparable to that found in the $[Pd_2\mathbf{A}_2\mathbf{CD}]^{4+}$ structure (14.33 Å).

After obtaining the $[Pd_2\mathbf{ABCD}]^{4+}$ isomer exclusively, we started to investigate the rationale leading to this remarkable selectivity. The dihedral angle $\angle\alpha$ between the $Pd(Py)_4$ planes in the structure was measured to be 21°, smaller than the angle for cage $[Pd_2\mathbf{A}_2\mathbf{CD}]^{4+}$ (33.9°), but indicating that shape-complementarity plays an important role as well. Although the selective formation of both cages $[Pd_2\mathbf{ABC}_2]^{4+}$ and $[Pd_2\mathbf{ABD}_2]^{4+}$ was found to be possible from the respective three-ligand mixtures, the clean assembly of cage $[Pd_2\mathbf{ABCD}]^{4+}$ from all four ligands again indicates a significant interligand contact between ligands **C** and **D**. Close inspection of the structure revealed that both of the geminal methyl groups on ligand **C** point to the π-surface of ligand **D** as discussed above for $[Pd_2\mathbf{A}_2\mathbf{CD}]^{4+}$ and $[Pd_2\mathbf{B}_2\mathbf{CD}]^{4+}$, forming C-H···π interactions with average distances of 2.9–3.1 Å, which is an even closer contact than found in the X-ray structure of $[Pd_2\mathbf{A}_2\mathbf{CD}]^{4+}$ in which only one of the methyl groups was found to interact with the neighboring ligand (compare Figs. 1 and 2b).

To probe the importance of the dimethyl C-H···π donor motif of ligand **C**, we performed a series of self-assembly control experiments by keeping ligands **A**, **B** and **D** the same but modifying the dimethyl motif of ligand **C** (Fig. 4a). First, ligand $\mathbf{D^1}$, which was formed by replacing the dimethyl group with an NH moiety, was combined with ligands **A**, **B**, **D**, and Pd^{II} for self-assembly, resulting in a convoluted NMR spectrum containing a mixture of more than four species (Supplementary Figs. 126 to 127). Then a similar ligand $\mathbf{D^2}$ with a $N\text{-}CH_3$ group was employed, which contains only one methyl group able to form C-H···π interactions. However, this again resulted in a complicated NMR spectrum, indicating a lack of self-sorting, although the MS spectrum showed cage $[Pd_2\mathbf{ABD^2D}]^{4+}$ as the major species (Supplementary Figs. 128 to 129). Remarkably, we managed to selectively crystallize cage $[Pd_2\mathbf{ABD^2D}]^{4+}$ out of this mixture (Supplementary Fig. 299). Although the structure clearly showed a C-H···π interaction directly from the methyl group of $\mathbf{D^2}$ towards the π-surface of ligand **D**, we suppose that the strength of this interaction is not strong enough to promote the selective formation of only one species. On the other hand, the methyl group in ligand $\mathbf{D^2}$ sits in plane with the ligand backbone, while the two methyl groups of ligand **C** protrude sideways from a sp^3-carbon center (Supplementary Figs. 125). To rule out an impact of the orientation effect on the strength of

the C-H···π interaction, we designed new ligand **D³** by replacing one of the two CH_3 motifs on the sp^3-carbon with a hydrogen substituent. Again, the according self-assembly revealed a complicated NMR spectrum (Supplementary Figs. 130 to 131), confirming that both of the methyl groups are crucial to the integrative self-sorting.

Next, we asked whether similar selective interactions also existed between ligands **A** and **B** in the $[Pd_2\mathbf{ABCD}]^{4+}$ system. However, ribbon-shaped ligand **A** adopts a rather bent conformation and is actually closer to ligand **D** than to **B** in the X-ray structure (Fig. 4 left). From a structural point of view, we can only speculate that exactly one count of ligand **A**, possessing a backbone with a spring-like flexibility (Pd-Pd distances in cages containing **A** vary between 13.66 and 15.94 Å), adjusts to the required length in combination with ligands **B**, **C** and **D**, while a pair of **A** leads to a too flexible and a pair of **B** to a too rigid assembly. Indeed, both experimentally obtained values from the reaction of $[Pd_2\mathbf{A}_2\mathbf{CD}]^{4+}$ plus $[Pd_2\mathbf{B}_2\mathbf{CD}]^{4+}$ to give 2x cage $[Pd_2\mathbf{ABCD}]^{4+}$ ($\Delta H = -19.5$ kJ mol^{-1}, $\Delta G = -11.7$ kJ mol^{-1}, see Fig. 5b and van't Hoff analysis in the Supplementary Information) as well as the DFT-calculated energy change (ωB97X-D/DEF2-SVP, $\Delta E = -10.1$ kJ mol^{-1}) point to a significant enthalpic driving force for combining ligands **A** and **B** within the same assembly.

To investigate the generality of forming heteroleptic cages with four different components we then screened further ligand variations. First, the replacement of ligand **B** with **B⁰**, containing an N-hexyl carbazole backbone also resulted in the exclusive formation of a similar cage $[Pd_2\mathbf{AB^0CD}]^{4+}$, supported by 1D, 2D NMR spectra and HR-ESI-MS (Supplementary Figs. 118 to 124). X-ray structure analysis revealed that the position of ligands **A**, **C**, and **D** in $[Pd_2\mathbf{AB^0CD}]^{4+}$ almost perfectly overlap with those in $[Pd_2\mathbf{ABCD}]^{4+}$, while the tendency of ligand **B⁰** to bent towards **A** is larger in the former case (Fig. 4b, Supplementary Figs. 298). Given that the dimethyl group on ligand **C** is indispensable to supporting strong enough C-H···π interactions to control the self-sorting, we then investigated if changing the π-surface of ligand **D** will also have an effect. We found that all ligands **D¹**, **D²**, or **D³** assemble with **A**, **B** and **C** to yield a clean NMR spectrum (Supplementary Figs. 168, 210 and 231). HR-ESI-MS confirmed the formation of corresponding heteroleptic cages with four different ligands. Trapped ion mobility spectrometry (ESI-TIMS-TOF) revealed only one narrow peak for each $[Pd_2\mathbf{ABCD^n}]^{4+}$ cage, excluding the formation of several isomers (Supplementary Fig. 289). NOESY correlations further supported the formation of a $[Pd_2\mathbf{ABCD^n}]^{4+}$ isomer (n =1–3) in all cases (Supplementary Figs. 171, 214 and 234). A crystal structure was obtained for cage $[Pd_2\mathbf{ABCD^2}]^{4+}$ and it almost perfectly superimposes with that of cage $[Pd_2\mathbf{ABCD}]^{4+}$

(Supplementary Figs. 298). These results suggest that a wide choice of ligands $\mathbf{D^n}$ with π-surface and suitable length is sufficient to achieve self-sorting.

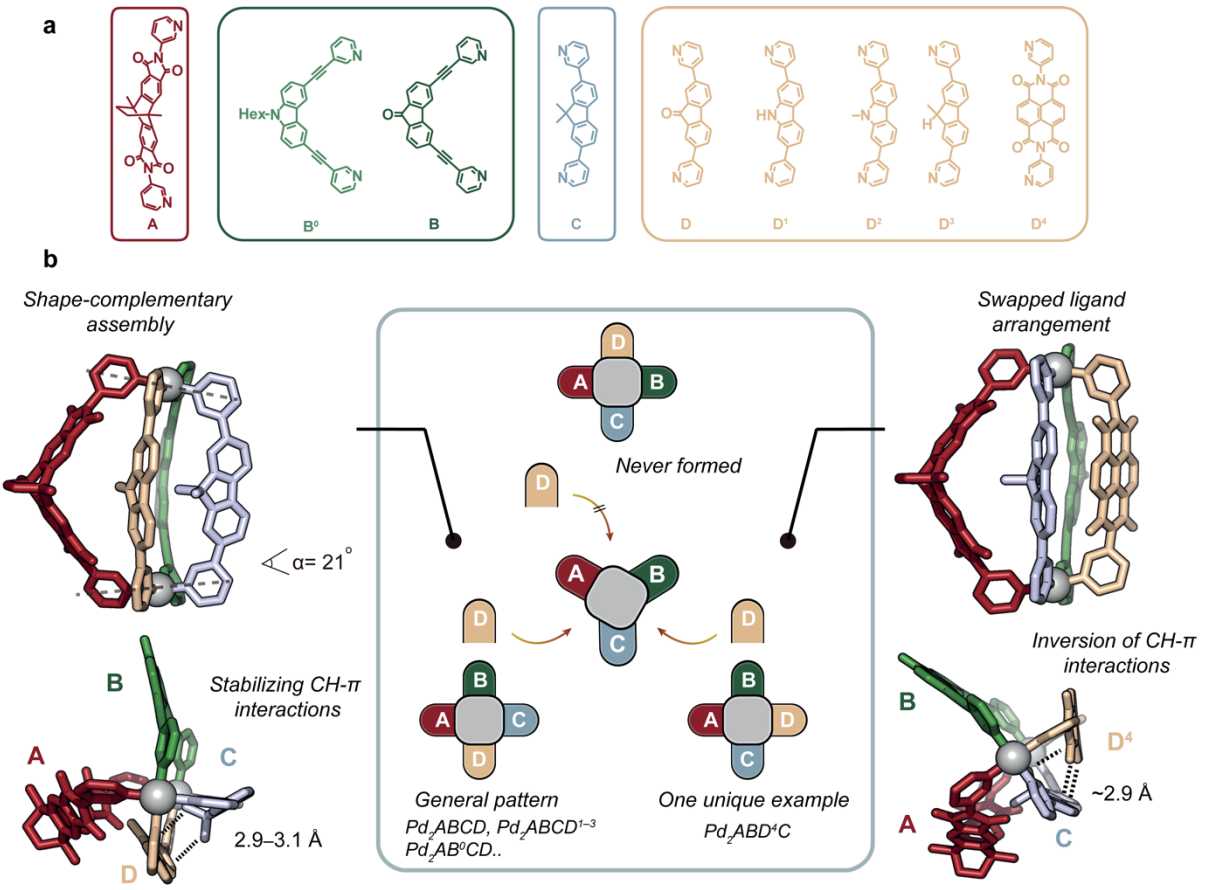

Fig. 4 | Possible cage isomers and comparison of crystal structures of [Pd₂ABCD] and [Pd₂ABD⁴C]. **a,** Used ligands. **b,** Left: side and top X-ray views of cage $[Pd_2\mathbf{ABCD}]^{4+}$ (dihedral angle ∠α between [Pd(Py)₄] planes and distances of C-H···π interactions between **C** and **D** assigned). Right: X-ray of $[Pd_2\mathbf{ABD^4C}]$ (C-H···π distance between ligands $\mathbf{D^4}$ and **C** given).

Next, we tested the combination of naphthalene diimide- (NDI) based ligand $\mathbf{D^4}$ with **A**, **B**, and **C** and again obtained a well-resolved NMR spectrum, very similar to that of $[Pd_2\mathbf{ABCD}]^{4+}$. HR-ESI-MS confirmed the formula $[2Pd^{II}+\mathbf{A}+\mathbf{B}+\mathbf{C}+\mathbf{D^4}]^{4+}$ (Supplementary Figs. 250 to 256). We initially expected this species to be the $[Pd_2\mathbf{ABCD^4}]^{4+}$ isomer, however, NOESY indicated a different ligand arrangement speaking for a $[Pd_2\mathbf{ABD^4C}]^{4+}$ ligand order by showing correlations between protons H7 of ligand **A** and **C**, and protons H7 of ligand **B** and $\mathbf{D^4}$ (Supplementary Figs. 254). The exclusive formation of a single species was supported by a ^{1}H DOSY experiment (Supplementary Figs. 255). Unambiguous proof to confirm the altered ligand order in cage $[Pd_2\mathbf{ABD^4C}]^{4+}$ came from X-ray structural analysis. The cage crystallizes

in the $P\bar{1}$ space group, with the asymmetric unit containing one cage molecule (Fig. 4b right). The Pd···Pd distance in the structure is 13.99 Å, slightly larger than that in $[Pd_2\mathbf{ABCD}]^{4+}$ due to the longer N–N distance in ligand $\mathbf{D^4}$ as compared to **D** (13.26 Å *vs.* 13.02 Å). Surprisingly, in contrast to the $[Pd_2\mathbf{ABCD}]^{4+}$ structure where the geminal methyl groups of **C** point to the π-surface of ligand **D**, in $[Pd_2\mathbf{ABD^4C}]^{4+}$, the NDI backbone of ligand **D** rotates in a way that instead of providing its π-surface, two C-H substituents now point to the π-surface of ligand **C** (C-H···π distances 2.82–3.02 Å). The same was observed in the X-ray structure of three-component cage $[Pd_2\mathbf{B}_2\mathbf{D^4C}]^{4+}$ (Fig. 2c).

Evolution of multicomponent heteroleptic cages

The exclusive formation of heteroleptic cages with two, three, and up to four different ligands upon mixing and heating their individual components (including a Pd^{II} salt) in solution indicates that all examined species are formed as the thermodynamically most stable products. We were thus interested to find out if they can be obtained progressively from their homoleptic or two-component heteroleptic precursors in stepwise cage-to-cage transformations. We investigated this along different routes (Fig. 1b), employing simple NMR-based mixing experiments as well as van't Hoff dissection of thermodynamic parameters and DFT computations (Fig. 5b).

On side of the homoleptic assemblies, both ligands **A** and **B** were previously reported to form lantern-shaped $[Pd_2L_4]$ cages[38,47], while ligands **C** and **D** form a mixture of $[Pd_3L_6]$ rings and $[Pd_4L_8]$ tetrahedra. Mixing and heating pairs of these homoleptic cage solutions (1:1 stoichiometry with respect to ligand count) led to the clean transformation into two-component cages $[Pd_2\mathbf{A}_2\mathbf{C}_2]^{4+}$, $[Pd_2\mathbf{A}_2\mathbf{D}_2]^{4+}$, $[Pd_2\mathbf{B}_2\mathbf{C}_2]^{4+}$, and $[Pd_2\mathbf{B}_2\mathbf{D}_2]^{4+}$ (going from level I to II in Fig. 1b and Supplementary Fig. 257). Further, mixing pairs of these two-component cages allowed to obtain three-component cages $[Pd_2\mathbf{A}_2\mathbf{CD}]^{4+}$, $[Pd_2\mathbf{ABC}_2]^{4+}$, $[Pd_2\mathbf{ABD}_2]^{4+}$ and $[Pd_2\mathbf{B}_2\mathbf{CD}]^{4+}$ (level II to III in Fig. 1b and Supplementary Figs. 272–279). Finally, cage $[Pd_2\mathbf{ABCD}]^{4+}$ could be obtained by either combining two-component-cages $[Pd_2\mathbf{A}_2\mathbf{C}_2]^{4+}$ with $[Pd_2\mathbf{B}_2\mathbf{D}_2]^{4+}$ or $[Pd_2\mathbf{A}_2\mathbf{D}_2]^{4+}$ with $[Pd_2\mathbf{B}_2\mathbf{C}_2]^{4+}$ (level II to IV in Fig. 1b and Supplementary Figs. 284–287) or three-component cages $[Pd_2\mathbf{A}_2\mathbf{CD}]^{4+}$ with $[Pd_2\mathbf{B}_2\mathbf{CD}]^{4+}$ or $[Pd_2\mathbf{ABC}_2]^{4+}$ with $[Pd_2\mathbf{ABD}_2]^{4+}$ (level III to IV in Fig. 1b and Supplementary Fig. 280–283). Besides these stepwise procedures (*routes i-iv* in Fig. 1b), it is also possible to form cage $[Pd_2\mathbf{ABCD}]^{4+}$ directly by mixing all four homoleptic assemblies (level I to IV; *route v* in Fig. 1b and Supplementary Fig. 268).

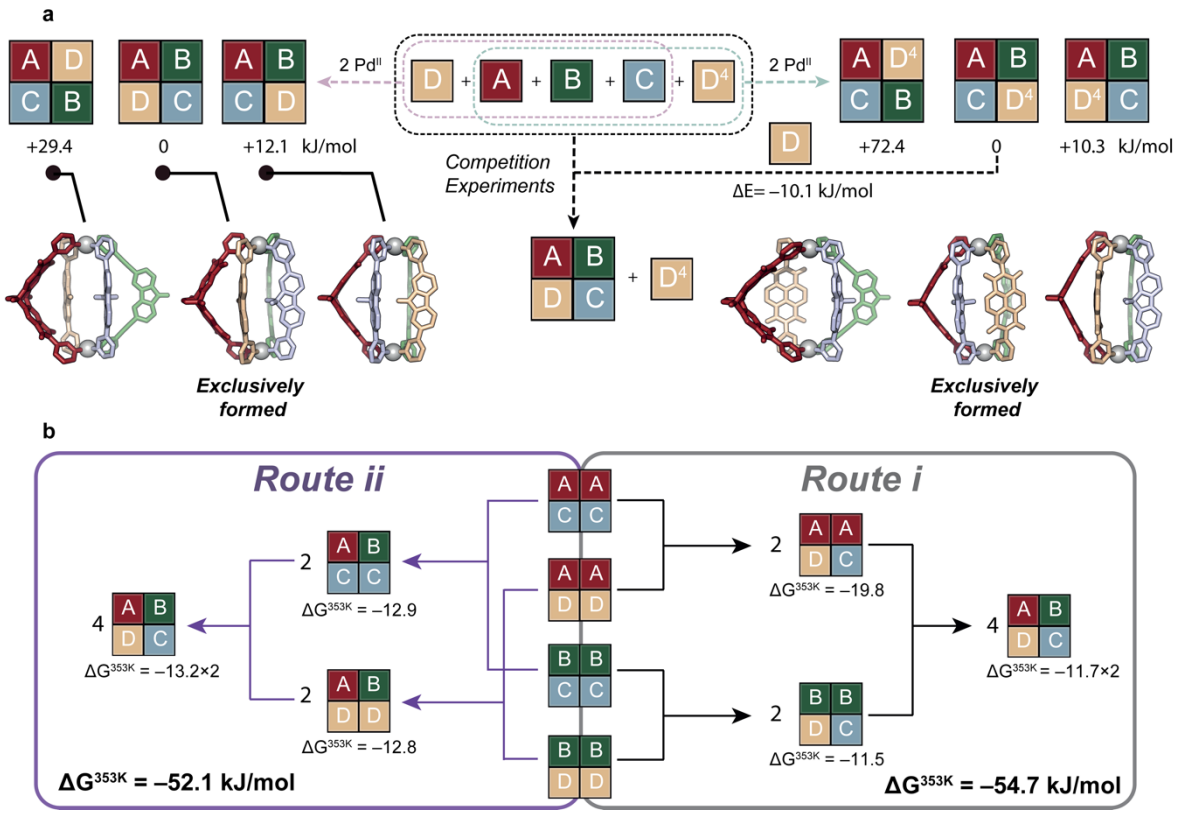

Fig. 5 | Thermodynamic analysis of cage isomers, competition experiments and sequential formation of [Pd$_2$ABCD]. a, Relative DFT-calculated energies and geometry-optimized structures of the three possible isomers formed from **A**, **B**, **C** plus **D** or **D^4**. Competition experiments showing preferential formation of [Pd$_2$**ABCD**]$^{4+}$ over [Pd$_2$**ABD^{4}C**]$^{4+}$ and calculated energetic difference. **b,** Formation of [Pd$_2$**ABCD**]$^{4+}$ via two different routes and measured free energy changes for each step.

For two routes, both starting from level II, we determined the Gibbs free energy changes for all cage-to-cage transformations by NMR-based equilibrium constant calculation (Fig. 5b) and further dissected the thermodynamic parameters by van't Hoff analyses, confirming that each step (from level II to III to IV) is energetically downhill. Notably, almost identical summed-up ΔG^{353K} values (–54.7 kJ/mol and –52.1 kJ/mol) were calculated for both routes towards cage [Pd$_2$**ABCD**]$^{4+}$ (Supplementary Figs. 286, Supplementary Table 2). In addition, kinetic data was obtained for a selection of cage-to-cage transformations by time-dependent NMR measurements, revealing that conversions from level II to III are faster when ligand **A** is contained instead of **B** (e.g [Pd$_2$**A**$_2$**C**$_2$]$^{4+}$ + [Pd$_2$**A**$_2$**D**$_2$]$^{4+}$ → 2 [Pd$_2$**A**$_2$**CD**]$^{4+}$: $t_{½}$ = 17.9 min vs. [Pd$_2$**B**$_2$**C**$_2$]$^{4+}$ + [Pd$_2$**B**$_2$**D**$_2$]$^{4+}$ → 2 [Pd$_2$**B**$_2$**CD**]$^{4+}$: $t_{½}$ = 41.5 min), which may again be explained by the higher structural flexibility of ligand **A**, facilitating ligand exchange from/to the square-planar Pd^{II} centers in the constrained 3D assembly. To rule out electronic influences, we compared structurally similar ligands **B** (electron-poor) and **B^0** (electron-rich) and found

virtually the same conversion kinetics, further supporting our assumption (Supplementary Figs. 258 to 267, Supplementary Table 1).

Subsequently, we looked deeper into the reasons for the observed ligand order in cages $[Pd_2\mathbf{ABCD}]^{4+}$ and $[Pd_2\mathbf{ABD^4C}]^{4+}$. Besides the qualitative arguments from inspection of the X-ray structures (discussed above), we computed the energies of all three possible isomers in both cases (cages with ligands **D** or $\mathbf{D^4}$, respectively) via DFT-based geometry optimizations and found that indeed the experimentally found isomers are also the energetically most favorable ones (Fig. 5a). A reason for the flipped ligand order in $[Pd_2\mathbf{ABCD}]^{4+}$ and $[Pd_2\mathbf{ABD^4C}]^{4+}$ can be deduced from comparing the electron rich/poor character of the directly interacting ligands via their electrostatic surface potential (ESP) maps (Supplementary Fig. 288), revealing that in the former case ligand **C** prefers to make CH_3-π interactions with the π-plane of ligand **D**. In $[Pd_2\mathbf{ABD^4C}]^{4+}$, however, the methyl groups of **C** refrain to point to the very positively polarized NDI-π surface of $\mathbf{D^4}$. Instead, the NDI CH substituents now point towards the π-surface of **C**. The resulting structural flip then seems to affect the shape-complementarity with the oppositely arranged ligands, leading to the observed change in the ligand order. Finally, we studied the stability difference between both four-component cages by performing a competitive experiment, i.e. introducing ligand **D** into the $[Pd_2\mathbf{ABD^4C}]^{4+}$ cage system which resulted in the disappearance of NMR signals of the original cage and the concurrent appearance of a new set of signals identical to that of cage $[Pd_2\mathbf{ABCD}]^{4+}$ (Supplementary Fig. 270). The preferable incorporation of ligand **D** over $\mathbf{D^4}$ could further be supported by calculating the ligand exchange via DFT (Fig. 5a).

Conclusion

A carefully chosen set of four different bis-monodentate ligands (**A**, **B**, **C** and **D**), all carrying the same kind of pyridyl donor groups, assemble with Pd^{II} cations to a single nanoscopic cage $[Pd_2\mathbf{ABCD}]^{4+}$ in a non-statistical fashion. Key for achieving this high degree of integrative self-sorting is the combination of ligand shape complementarity, balance of strain and interligand C-H···π interactions. We demonstrate the modular replacement of ligands, even allowing to control the ligand order around the metal nodes (as in $[Pd_2\mathbf{ABD^4C}]^{4+}$). This paves the way for further derivatization to embed functionality. As the assembly proceeds under full thermodynamic control, formed products are robust and produced in a reproducible manner, following several alternative routes (directly from ligands and Pd^{II}, by mixing homoleptic assemblies or stepwise via two- and three-component cages). Along these routes, more than 15 new heteroleptic cages were characterized, including nine X-ray structures. Just recently,

rational self-assembly strategies push the field of supramolecular architecture to vastly increase complexity beyond homoleptic structures (one type of ligand per assembly) and bring multiple components together in an integrative way. With the presented methodology, we have maximized the degree of ligand differentiation within the Pd^{II}-cage family with the lowest nuclearity, allowing to selectively form one out of 55 possible products. As a general concept, this will allow for the modular development of multifunctional assemblies in which the interplay of different components leads to emerging properties, attractive for applications in selective recognition, cooperative catalysis and materials science.

Methods

Self-assembly of $[Pd_2B_2C_2](BF_4)_4$.

To a solution of **C** (120 µL, 3 mM, 0.36 µmol) and a suspension of **B** (120 µL, 3 mM, 0.36 µmol) in CD_3CN were added a stock solution of $[Pd(CH_3CN)_4](BF_4)_2$ (24 µL, 15 mM/CD_3CN, 0.36 µmol) and 186 µL CD_3CN. The mixture was heated in a NMR tube at 80 °C for 8 h to give a 0.4 mM cage solution.

^{1}H NMR (500 MHz, 298 K, CD_3CN) δ 9.55 (d, *J* = 2.0 Hz, 4H), 9.43 (d, *J* = 1.8 Hz, 4H), 9.12 (dd, *J* = 5.9, 1.4 Hz, 4H), 9.02 (d, *J* = 5.8 Hz, 4H), 8.25 – 8.21 (m, 4H), 8.18 (dt, *J* = 8.1, 1.6 Hz, 4H), 7.95 (d, *J* = 7.7 Hz, 4H), 7.77 (s, 4H), 7.72 – 7.64 (m, 16H), 7.57 (d, *J* = 1.7 Hz, 4H), 7.49 (dd, *J* = 7.8, 1.7 Hz, 4H), 1.63 (s, 6H), 1.29 (s, 6H).

^{13}C NMR (176 MHz, 298 K, CD_3CN) δ 192.17, 156.86, 153.88, 151.25, 150.58, 150.16, 144.76, 144.73, 143.14, 140.66, 139.71, 136.11, 135.99, 135.52, 128.95, 128.87, 128.44, 128.31, 125.24, 124.25, 123.74, 122.93, 122.70, 95.43, 87.58, 48.26, 29.84, 25.86.

HR-ESI-MS $[BF_4+Pd_2\mathbf{B}_2\mathbf{C}_2]^{3+}$: *m/z* measured: 587.1211, calculated: 587.1200.

Self-assembly of $[Pd_2ABCD](BF_4)_4$.

To a solution of **A** (60 µL, 3 mM, 0.18 µmol), **C** (60 µL, 3 mM, 0.18 µmol) and a suspension of **B** (60 µL, 3 mM, 0.18 µmol), **D** (60 µL, 3 mM, 0.18 µmol) were added a stock solution of $[Pd(CH_3CN)_4](BF_4)_2$ (24 µL, 15 mM/CD_3CN, 0.36 µmol) and 186 µL CD_3CN. The mixture was heated in a NMR tube at 80 °C for 8 h to give a 0.4 mM cage solution.

^{1}H NMR (700 MHz, 298 K, CD_3CN) δ 9.89 (d, *J* = 2.1 Hz, 2H), 9.38 (t, *J* = 2.7 Hz, 4H), 9.25 (d, *J* = 1.9 Hz, 2H), 9.16 (d, *J* = 5.9 Hz, 2H), 9.02 (d, *J* = 5.8 Hz, 2H), 8.97 (d, *J* = 5.8 Hz, 2H), 8.71 (d, *J* = 6.0 Hz, 2H), 8.53 (d, *J* = 1.8 Hz, 2H), 8.40 (d, *J* = 7.8 Hz, 2H), 8.17 – 8.10 (m, 4H), 8.00 (d, *J* = 7.5 Hz, 2H), 7.90 – 7.86 (m, 4H), 7.85 (d, *J* = 7.7 Hz, 2H), 7.79 (s, 2H), 7.75 –

7.69 (m, 6H), 7.65 – 7.61 (m, 4H), 7.61 – 7.59 (m, 2H), 7.48 (s, 2H), 7.46 (dd, J = 7.6, 1.8 Hz, 2H), 7.09 (d, J = 1.8 Hz, 2H), 2.12 (s, 3H), 1.97 (s, 3H), 1.81 (s, 4H), 1.32 (s, 3H), 0.55 (s, 3H). **^{13}C NMR** (151 MHz, 298 K, CD_3CN) δ 194.28, 192.81, 173.03, 167.76, 167.65, 167.11, 166.94, 154.71, 154.63, 153.97, 151.26, 151.15, 150.50, 150.43, 150.32, 149.86, 149.83, 145.99, 144.74, 142.35, 142.03, 140.18, 139.66, 139.08, 138.48, 138.42, 137.29, 136.69, 136.23, 135.69, 135.46, 131.86, 130.66, 130.58, 128.69, 128.49, 128.38, 128.34, 127.92, 125.13, 124.89, 124.07, 123.64, 123.44, 123.05, 122.69, 117.56, 95.28, 87.38, 46.85, 45.04, 32.64, 30.37, 27.10, 23.39, 18.75, 14.39.

HR-ESI-MS $[BF_4+Pd_2\mathbf{ABCD}]^{3+}$: *m/z* measured: 630.4541, calculated: 630.4539.

Data availability statement

Crystallographic data for the structures reported in this paper have been deposited at the Cambridge Crystallographic Data Centre, under the deposition numbers 2207621 *trans*-$[Pd_2\mathbf{A}_2\mathbf{B}_2](BF_4)_4$, 2207622 $[Pd_2\mathbf{B}_2\mathbf{CD}^1](BF_4)_4$, 2207623 $[Pd_2\mathbf{A}_2\mathbf{CD}](BF_4)_4$, 2207624 $[Pd_2\mathbf{B}_2\mathbf{D}^4\mathbf{C}](BF_4)_4$, 2207625 $[Pd_2\mathbf{ABCD}](BF_4)_4$, 2207626 $[Pd_2\mathbf{AB}^0\mathbf{CD}](BF_4)_4$, 2207627 $[Pd_2\mathbf{ABD}^4\mathbf{C}](BF_4)_4$, 2207628 $[Pd_2\mathbf{ABD}^2\mathbf{D}](BF_4)_4$, 2207629 $[Pd_2\mathbf{ABCD}^2](BF_4)_4$. Copies of these data can be obtained free of charge via www.ccdc.cam.ac.uk/data_request/cif. All other data supporting the findings of this study are available within the Article and its Supplementary Information, or from the corresponding author upon reasonable request.

Acknowledgments

We thank the European Research Council (ERC Consolidator grant 683083, RAMSES) for financial support. This work was funded by the Deutsche Forschungsgemeinschaft (DFG, German Research Foundation) under Germany's Excellence Strategy EXC 2033 “RESOLV”, project number 390677874, and GRK2376 “Confinement-controlled Chemistry”, project number 331085229. The authors thank Dr. Bin Chen, Dr. Jacopo Tessarolo, André Platzek, Kristina Ebbert and Dr. Shota Hasegawa for providing ligands and Laura Schneider for ESI mass spectra measurements. We thank Dr. Julian J. Holstein for helpful suggestions on the crystallographic data analysis.

Author contributions

K.W. and G.H.C conceived the project and wrote the manuscript together with E.B. K.W. performed the experiments and analyzed the data. A.B. provided ion-mobility mass measurements. K.W. collected the X-ray single-crystal data and refined the crystal structures.

Competing Interests

The authors declare no competing interests.

References

1. Kelly, J. A., Sielecki, A. R., Sykes, B. D., James, M. N. G. & Phillips, D. C. X-ray crystallography of the binding of the bacterial cell wall trisaccharide NAM-NAG-NAM to lysozyme. *Nature* **282**, 875–878 (1979).
2. Ringe, D. & Petsko, G. A. How Enzymes Work. *Science* **320**, 1428–1429 (2008).
3. Liu, M. et al. Barely porous organic cages for hydrogen isotope separation. *Science* **366**, 613–620 (2019).
4. Cook, T. R. & Stang, P. J. Recent Developments in the Preparation and Chemistry of Metallacycles and Metallacages via Coordination. *Chem. Rev.* **115**, 7001–7045 (2015).
5. Fujita, M. et al. Self-assembly of ten molecules into nanometre-sized organic host frameworks. *Nature* **378**, 469–471 (1995).
6. Mal, P., Breiner, B., Rissanen, K. & Nitschke, J. R. White Phosphorus Is Air-Stable Within a Self-Assembled Tetrahedral Capsule. *Science* **324**, 1697–1699 (2009).
7. Zhang, D., Ronson, T. K., Zou, Y.-Q. & Nitschke, J. R. Metal–organic cages for molecular separations. *Nat. Rev. Chem.* **5**, 168–182 (2021).
8. Galan, A. & Ballester, P. Stabilization of reactive species by supramolecular encapsulation. *Chem. Soc. Rev.* **45**, 1720–1737 (2016).
9. Brown, C. J., Toste, F. D., Bergman, R. G. & Raymond, K. N. Supramolecular Catalysis in Metal–Ligand Cluster Hosts. *Chem. Rev.* **115**, 3012–3035 (2015).
10. Chen, L.-J., Yang, H.-B. & Shionoya, M. Chiral metallosupramolecular architectures. *Chem. Soc. Rev.* **46**, 2555–2576 (2017).
11. Brzechwa-Chodzyńska, A., Drożdż, W., Harrowfield, J. & Stefankiewicz, A. R. Fluorescent sensors: A bright future for cages. *Coord. Chem. Rev.* **434**, 213820 (2021).
12. Goeb, S. & Sallé, M. Electron-rich Coordination Receptors Based on Tetrathiafulvalene Derivatives: Controlling the Host–Guest Binding. *Acc. Chem. Res.* **54**, 1043–1055 (2021).
13. Wu, K. et al. The Redox Coupling Effect in a Photocatalytic Ru^{II}-Pd^{II} Cage with TTF Guest as Electron Relay Mediator for Visible-Light Hydrogen-Evolving Promotion. *Angew. Chem. Int. Ed.* **59**, 2639–2643 (2020).
14. Wezenberg, S. J. Light-switchable Metal-Organic Cages. *Chem. Lett.* **49**, 609–615 (2020).
15. Li, R.-J., Tessarolo, J., Lee, H. & Clever, G. H. Multi-stimuli Control over Assembly and Guest Binding in Metallo-supramolecular Hosts Based on Dithienylethene Photoswitches. *J. Am. Chem. Soc.* **143**, 3865–3873 (2021).
16. Chakrabarty, R., Mukherjee, P. S. & Stang, P. J. Supramolecular Coordination: Self-Assembly of Finite Two- and Three-Dimensional Ensembles. *Chem. Rev.* **111**, 6810–6918 (2011).
17. Fujita, D. et al. Self-assembly of tetravalent Goldberg polyhedra from 144 small components. *Nature* **540**, 563–566 (2016).
18. Wu, K., Tessarolo, J., Baksi, A. & Clever, G. H. Guest-Modulated Circularly Polarized Luminescence by Ligand-to-Ligand Chirality Transfer in Heteroleptic PdII Coordination Cages. *Angew. Chem. Int. Ed.* **61**, e202205725 (2022).
19. Frank, M. et al. Light-Induced Charge Separation in Densely Packed Donor–Acceptor Coordination Cages. *J. Am. Chem. Soc.* **138**, 8279–8287 (2016).

20. García-Simón, C. et al. Enantioselective Hydroformylation by a Rh-Catalyst Entrapped in a Supramolecular Metallocage. *J. Am. Chem. Soc.* **137**, 2680–2687 (2015).
21. Wang, Q.-Q. et al. Self-assembled nanospheres with multiple endohedral binding sites pre-organize catalysts and substrates for highly efficient reactions. *Nat. Chem.* **8**, 225–230 (2016).
22. Howlader, P., Das, P., Zangrando, E. & Mukherjee, P. S. Urea-Functionalized Self-Assembled Molecular Prism for Heterogeneous Catalysis in Water. *J. Am. Chem. Soc.* **138**, 1668–1676 (2016).
23. Pruchyathamkorn, J. et al. A Complex Comprising a Cyanine Dye Rotaxane and a Porphyrin Nanoring as a Model Light-Harvesting System. *Angew. Chem. Int. Ed.* **59**, 16455–16458 (2020).
24. Wang, W. et al. The construction of complex multicomponent supramolecular systems via the combination of orthogonal self-assembly and the self-sorting approach. *Chem. Sci.* **5**, 4554–4560 (2014).
25. Kramer, R., Lehn, J. M. & Marquis-Rigault, A. Self-recognition in helicate self-assembly: spontaneous formation of helical metal complexes from mixtures of ligands and metal ions. *Proc. Natl. Acad. Sci. USA* **90**, 5394–5398 (1993).
26. Sauvage, J. P. & Weiss, J. Synthesis of biscopper(I) [3]-catenates: multiring interlocked coordinating systems. *J. Am. Chem. Soc.* **107**, 6108–6110 (1985).
27. Kumazawa, K., Biradha, K., Kusukawa, T., Okano, T. & Fujita, M. Multicomponent Assembly of a Pyrazine-Pillared Coordination Cage That Selectively Binds Planar Guests by Intercalation. *Angew. Chem. Int. Ed.* **42**, 3909–3913 (2003).
28. Zheng, Y.-R. et al. A Facile Approach toward Multicomponent Supramolecular Structures: Selective Self-Assembly via Charge Separation. *J. Am. Chem. Soc.* **132**, 16873–16882 (2010).
29. Wessjohann, L. A., Kreye, O. & Rivera, D. G. One-Pot Assembly of Amino Acid Bridged Hybrid Macromulticyclic Cages through Multiple Multicomponent Macrocyclizations. *Angew. Chem. Int. Ed.* **56**, 3501–3505 (2017).
30. He, Z., Jiang, W. & Schalley, C. A. Integrative self-sorting: a versatile strategy for the construction of complex supramolecular architecture. *Chem. Soc. Rev.* **44**, 779–789 (2015).
31. Pullen, S., Tessarolo, J. & Clever, G. H. Increasing structural and functional complexity in self-assembled coordination cages. *Chem. Sci.* **12**, 7269–7293 (2021).
32. Sun, Q.-F., Sato, S. & Fujita, M. An $M_{12}(L^1)_{12}(L^2)_{12}$ Cantellated Tetrahedron: A Case Study on Mixed-Ligand Self-Assembly. *Angew. Chem. Int. Ed.* **53**, 13510–13513 (2014).
33. Bloch, W. M. et al. Geometric Complementarity in Assembly and Guest Recognition of a Bent Heteroleptic *cis*-$[Pd_2L^A_2L^B_2]$ Coordination Cage. *J. Am. Chem. Soc.* **138**, 13750–13755 (2016).
34. Sudan, S. et al. Identification of a Heteroleptic $Pd_6L_6L'_6$ Coordination Cage by Screening of a Virtual Combinatorial Library. *J. Am. Chem. Soc.* **143**, 1773–1778 (2021).
35. Li, J.-R. & Zhou, H.-C. Bridging-ligand-substitution strategy for the preparation of metal–organic polyhedra. *Nat. Chem.* **2**, 893–898 (2010).
36. Prusty, S., Yazaki, K., Yoshizawa, M. & Chand, D. K. A Truncated Molecular Star. *Chem. Eur. J.* **23**, 12456–12461 (2017).
37. Yamashina, M., Yuki, T., Sei, Y., Akita, M. & Yoshizawa, M. Anisotropic Expansion of an M_2L_4 Coordination Capsule: Host Capability and Frame Rearrangement. *Chem. Eur. J.* **21**, 4200–4204 (2015).

38. Chen, B., Holstein, J. J., Horiuchi, S., Hiller, W. G. & Clever, G. H. Pd(II) Coordination Sphere Engineering: Pyridine Cages, Quinoline Bowls, and Heteroleptic Pills Binding One or Two Fullerenes. *J. Am. Chem. Soc.* **141**, 8907–8913 (2019).
39. Preston, D., Barnsley, J. E., Gordon, K. C. & Crowley, J. D. Controlled Formation of Heteroleptic $[Pd_2(L_a)_2(L_b)_2]^{4+}$ Cages. *J. Am. Chem. Soc.* **138**, 10578–10585 (2016).
40. Ogata, D. & Yuasa, J. Dynamic Open Coordination Cage from Nonsymmetrical Imidazole–Pyridine Ditopic Ligands for Turn-On/Off Anion Binding. *Angew. Chem. Int. Ed.* **58**, 18424–18428 (2019).
41. Lewis, J. E. M., Tarzia, A., White, A. J. P. & Jelfs, K. E. Conformational control of Pd_2L_4 assemblies with unsymmetrical ligands. *Chem. Sci.* **11**, 677–683 (2020).
42. Tessarolo, J., Lee, H., Sakuda, E., Umakoshi, K. & Clever, G. H. Integrative Assembly of Heteroleptic Tetrahedra Controlled by Backbone Steric Bulk. *J. Am. Chem. Soc.* **143**, 6339–6344 (2021).
43. De, S., Mahata, K. & Schmittel, M. Metal-coordination-driven dynamic heteroleptic architectures. *Chem. Soc. Rev.* **39**, 1555–1575 (2010).
44. Johnson, A. M. & Hooley, R. J. Steric Effects Control Self-Sorting in Self-Assembled Clusters. *Inorg. Chem.* **50**, 4671–4673 (2011).
45. Liu, Y. et al. Controlled Construction of Heteroleptic $[Pd_2(L^A)_2(L^B)(L^C)]^{4+}$ Cages: A Facile Approach for Site-Selective endo-Functionalization of Supramolecular Cavities. *Angew. Chem. Int. Ed.* **62**, e202217215 (2023).
46. Wu, K., Zhang, B., Drechsler, C., Holstein, J. J. & Clever, G. H. Backbone-Bridging Promotes Diversity in Heteroleptic Cages. *Angew. Chem. Int. Ed.* **60**, 6403–6407 (2021).
47. Ebbert, K. E. et al. Resolution of minor size differences in a family of heteroleptic coordination cages by trapped ion mobility ESI-MS. *Dalton Trans.* **48**, 11070–11075 (2019).